Characterizing the microscopic physics near moving contact lines using dynamic contact angle data

E. Ramé
National Center for Microgravity Research (NCMR), c/o NASA Glenn Research Center, MS 110-3, Cleveland, Ohio 44135, USA

S. Garoff*
Department of Physics and Center for Complex Fluids Engineering, Carnegie Mellon University, Pittsburgh, Pennsylvania 15213, USA

K. R. Willson†
Department of Physics, Carnegie Mellon University, Pittsburgh, Pennsylvania 15213, USA
(Received 10 March 2004; published 29 September 2004)

Directly probing the fluid flow and liquid-vapor interface shape in the microscopic immediate vicinity of the moving contact line can only be accomplished in very specific and isolated cases. Yet this physics is critical to macroscopic dynamic wetting. Here we examine the microscopic (or inner) physics of spreading silicone fluids using data of macroscopic dynamic contact angle versus Capillary number $\mathrm{Ca}=U\mu/\sigma$. This dynamic contact angle is precisely defined so that it can be related back to the microscopic behavior through detailed theory. Our results indicate that the parameters describing the inner region have a detectable dependence on spreading velocity when this velocity exceeds a critical value. This dependence is not scaled (i.e., the data are not collapsed) by Ca, which suggests that an additional time scale must be present in the model of the inner region.

DOI: 10.1103/PhysRevE.70.031608 PACS number(s): 68.08.Bc, 68.03.Kn, 68.03.Cd

I. INTRODUCTION

Wetting dynamics is intimately related to the motion of a fluid in the highly confined region in the immediate vicinity of the moving contact line. The laws that control the fluid motion in that region (called the "inner region," see below) are different from those that govern the motion of the bulk material farther from the contact line [1–3]. Since experimentally probing the inner region directly has as yet been impossible in almost all cases, efforts to determine the inner scale physics use measurement of some larger-scale feature (usually the dynamic contact angle) and then relate the measurements back to the inner physics using theories.

The literature on dynamic contact angles displays a great lack of uniformity on the definition and measurement of this quantity, on how to translate the measurement from one geometry to another [4], and on the correct method of extracting information on the inner scale physics using the measured quantity. The chief difficulty is that geometry-independent, material-only-dependent dynamic contact angles cannot be measured directly; hence they must be inferred by interpreting the measurement of some other physical quantity. Despite this problem, much useful information on the hydrodynamics in the region neighboring, but not including, the contact line has been extracted using somewhat disparate (or inconsistent) physical measurements [5–7].

Near a contact line moving relative to a solid with speed U, the flow of a Newtonian fluid of viscosity μ and surface tension σ obeying the no-slip condition at the solid exhibits a nonintegrable stress singularity. This singularity prevents one from satisfying a contact angle condition at the moving contact line [1]. To remedy this failure of the model, it has been assumed that, within a distance L_i of the contact line (called the "inner" region), new mechanisms (e.g., liquid slip at the solid [8–10] or a shear-thinning viscosity [11]) are present that remove the singularity. One can then specify that the angle θ between the solid and the local tangent to the interface satisfies $\theta=\Theta_i$ at the contact line. Hydrodynamic analyses [12–14] relate the macroscopic dynamic contact angle θ_d measurable in an outer or macroscopic length, L_{out}, to the inner or actual contact angle, Θ_i, an inner length scale, L_i, and the capillary number $\mathrm{Ca}(=U\mu/\sigma)$,

$$g(\theta_d) = g(\Theta_i) + \mathrm{Ca}\,\ln(L_{\mathrm{out}}/L_i), \tag{1}$$

where $g(x)\equiv\int_0^x\{(y-\cos y\,\sin y)/2\,\sin y\}dy$ when the second fluid is assumed to be a gas whose dynamics may be ignored [42]. As we discuss below in Sec. II A, θ_d need not be the interface slope at any particular location.

The physics of the inner region is of considerable intrinsic interest. Further, to the extent that it has an impact on the macroscopic contact angle [as illustrated by Eq. (1)] and flow fields, it controls the macroscopic dynamic wetting seen in nature and used in a wide variety of technologies. However, there have been no direct experimental measurements of the nature of the mechanism that removes the singularity. While very careful measurements of spreading over precursing films provide useful information about macroscopic spreading, they do not address how the singularity is removed at the actual contact line [15,16]. In fact, it is not even guaranteed that the singularity should be removed by mechanisms at the continuum scale; for example, the models by

*Corresponding author:
Electronic address: sg2e@andrew.cmu.edu
†Present address: Southwest Research Institute, 6220 Culebra Road, San Antonio, TX 78238, USA.

Blake and collaborators consider the hopping of molecules at the contact line [3].

Elucidating the inner physics is challenging. Even the much more limited goal of getting values of Θ_i and L_i at each velocity poses significant problems. In fact, Eq. (1) shows that macroscopic measurements of θ_d can only yield $g(\Theta_i) - \mathrm{Ca}\ \ln(L_i)$, i.e., not the individual values of Θ_i and L_i at each spreading velocity U [4,17,18]. An approach taken in the past to deal with this situation has been to ignore the U dependence and assume that Θ_i and L_i are constants. This implies that Θ_i would equal the static contact angle, θ_s. Then L_i may be deduced by fitting Eq. (1) to data of θ_d versus Ca [13]. Of course this approach is arbitrary. The theory leading to Eq. (1) does not require Θ_i or L_i to be constants, nor is there experimental evidence that they are constants. In fact, our results indicate that either one or both of Θ_i and L_i depend on U, a situation wholly compatible with all of the assumptions that lead to Eq. (1).

The only approach based on first principles to address inner physics is molecular-dynamics (MD) simulations. Since the late 1980s, these simulations have opened a window into the inner region by suggesting that the liquid adjacent to the solid may slip within a few molecular diameters from the contact line [19,20]. Using MD simulations with typical Lennard-Jones potentials, Hadjiconstantinou [21] recently found a slip velocity that he fitted with an exponential decay of about two molecular lengths from the contact line. This investigation is unique in that it attempts to connect this microscopic analysis to a continuum hydrodynamic analysis. Based on the agreement with finite-element calculations that incorporate the slip condition found in the MD simulation and use the static value for Θ_i, it is suggested that Θ_i is almost equal to the static equilibrium angle, θ_s. Similar conclusions are derived in MD simulations by De Conink and collaborators, who extract an apparent dynamic contact angle and interpret its value in terms of Blake's molecular kinetic model of the inner physics [22]. However, other MD simulations by Jin, Koplik, and Banavar [23] suggest that Θ_i does vary with spreading velocity. On the other hand, theoretical investigations that probe the velocity dependence of Θ_i and L_i are scarce. Among these, we note the diffuse interface model analysis of Chen *et al.* [24] that predicts a velocity-dependent L_i not scalable by Ca and Eggers and Stone's [25] new look at the lubrication equations that yields a cutoff length for the logarithmic singularity proportional to Ca^{α} when a meniscus advances over a film.

In the analysis of $\theta(U)$ for certain experiments, the assumption $\Theta_i = \theta_s$ applied to Eq. (1) has generated values for L_i that are below molecular dimensions. These unphysically small values of L_i have led some [26] to suggest that a significant extra source of dissipation must be present near the contact line in addition to the viscous flow outside the inner region. This conclusion need not be valid if the analysis of the experimental data allows Θ_i and L_i to be functions of U. If a suitable (not yet known) dependence for $\Theta_i(U)$ is used in the analysis of the experimental data, L_i may be brought to physically reasonable ranges.

The objective of this study is to establish whether there is dynamic variation in Θ_i and L_i as well as whether this variation is only of a hydrodynamic origin, i.e., whether the U dependence can be described by the single parameter Ca. This latter aspect is crucial because the lack of Ca scalability would indicate that other time scales arising from L_i and a new velocity scale (needed to nondimensionalize the non-Ca dependence on U) are acting in the inner region. The possibility of other time scales is not a new idea: they may arise because molecular rearrangements are not instantaneous. Shikhmurzaev has used this concept in his model where material mapped from the liquid-gas to the solid-liquid interface as the contact line moves does not attain its equilibrium solid-liquid surface energy until a (relaxation) time τ_{rel} after the material has passed by the contact line region [27,28].

In Sec. II, we discuss the general requirements of hydrodynamic theories, showing a precise definition of the dynamic contact angle and that the inner parameters may depend on velocity. In Sec. III, we discuss our experimental methods, emphasizing the detailed and accurate fitting of the data and thus the validity of extracting inner parameters using Eq. (1). In Sec. IV, we discuss our results on a suite of systems, showing that inner scale parameters carefully extracted can give intriguing new insight into inner scale dynamics.

II. ESSENCE OF THE MODELS

A. General remarks on the models

1. Approaches based on dissipation

A formulation which balances the rate of viscous dissipation with the rate of work done by the driving force of the contact line is often used to connect the microscopic phenomena near the contact line with a macroscopically defined contact angle and its velocity dependence. If one neglects the change of the liquid-vapor interface area due to interfacial viscous deformation outside of the inner region, then the driving force is proportional to $\cos\theta_d - \cos\theta_s$ [29]. Using the small-slope approximation and setting $\theta_s = 0$ lead to the power law $\theta_d \sim \mathrm{Ca}^{1/3}$ in agreement with the small-Ca limit of Eq. (1) when $\Theta_i = 0$ and L_i is independent of U. One may find the dissipation away from the inner region (where the physics is known) from the flow calculated in a particular fluid body. If one considers that dissipation in the inner region must be accounted for, then one must include another term of dissipation [30].

The dissipation-based approach is by nature an "integral" balance. As such, it does not inform about the detailed deformation of the interface by viscous forces but it can in principle yield the correct parametric dependence for θ_d. However, in cases where the inner dissipation is small compared to that in the rest of the fluid body, caution must be observed in using these methods. The dissipation away from the contact line must be calculated extremely accurately or errors in that calculation will lead directly to errors in the estimation of the inner physics. Further, it would be extremely difficult to verify experimentally that the dissipation away from the contact line is calculated correctly so that one has experimental verification that the inner physics is inferred accurately from a measurement of θ_d versus Ca.

2. Approach based on hydrodynamic analysis

In this study, we take a more detailed approach to probing the inner scale physics. Our study is based on solutions of

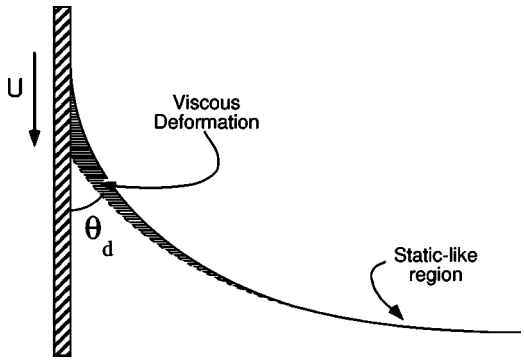

FIG. 1. Schematic showing the intermediate region (horizontally dashed) where viscous deformation is significant. Far from the contact line, the interface is staticlike because $\mathrm{Ca} \ll 1$ and viscous forces are negligible compared to surface tension. The extrapolation of the staticlike region back to the solid makes an "apparent" contact angle θ_d with the solid.

the flow fields and interface shapes near the moving contact line using the systematic asymptotic method of Cox [12]. Besides relating θ_d to Θ_i, L_i, and Ca, this theory also predicts the functional form of the interface deformation by viscous stresses near the contact line. This deformation largely determines the dynamic contact angle θ_d, the effective boundary condition for the interface shape far from the contact line. This model of the functional form of the interface deformation has been shown to be accurate for a suite of relatively viscous simple polymeric fluids [17,31]. In the present study, we extract information about the inner physics only after experimentally verifying that the asymptotic model describes very accurately the viscous deformation of the interface near the contact line. As we will show, this precaution is critical to getting sufficiently well defined and precisely determined contact angles that inner scale physics can be exposed. Simpler methods for determining θ_d could lead to large errors in revealing the inner physics.

Since our experimental results will depend on the use of Eq. (1), we examine briefly the assumptions behind the model that produces it. The key in the development of Eq. (1) is that no assumption is made about the velocity dependence of the inner parameters, Θ_i, L_i. Thus, in general they may depend either locally on spreading velocity U or possibly even nonlocally on some other macroscopic characteristic of the flow field [32]. The single physical assumption for the inner region is that a suitable (but unspecified) mechanism exists with characteristic length L_i that removes the singularity [12].

Neglecting gravity and inertia, the dimensionless groups Ca and $\epsilon \equiv L_i/L_{\mathrm{out}}$ describe the flow in the vicinity of the contact line. The limit $\mathrm{Ca} \to 0$ holding $\mathrm{Ca} \ln \epsilon = -A$ $(A>0)$ fixed yields Eq. (1) as the main result. This limit process establishes a specific order relation between Ca and ϵ, which implies that $\epsilon \to 0$ in a specific way, i.e., $\epsilon = \exp(-A/\mathrm{Ca})$ as $\mathrm{Ca} \to 0$. An O(1) independent variable is defined as $\xi \equiv \mathrm{Ca} \ln(r/L_{\mathrm{out}})$. Consequently, for ξ fixed and O(1), the physical distance from the contact line, r, satisfies $r/L_{\mathrm{out}} \ll 1$ and $r/L_i \gg 1$. Thus, the region where $\xi = \mathrm{O}(1)$ lies between the inner and the outer and is called "intermediate." The two chief features of the intermediate region are (i) the flow and interface shape are independent of the system geometry, and (ii) viscous and surface tension forces balance even though $\mathrm{Ca} \ll 1$. The interface shape, specified by the slope of the interface, θ, in the intermediate and beginning of the outer regions is given by [18]

$$\theta \sim g^{-1}\left(g(\theta_d) + \mathrm{Ca} \ln \frac{r}{L_{\mathrm{out}}}\right) + f_0(r/L_{\mathrm{out}}; \theta_d) - \theta_d \quad \text{as } r/L_{\mathrm{out}} \to 0, \tag{2}$$

where g^{-1} denotes the inverse function of g, $g^{-1}(g(x)) = x$, and $f_0(r/L_{\mathrm{out}}; \theta_d)$ represents the equation of a static meniscus with contact angle θ_d, i.e., $\theta_d = f_0(0; \theta_d)$, see Fig. 1.

The first term on the right-hand side of Eq. (2) accounts for the viscous deformation of the interface in the intermediate region discussed above. It depends only on the inner region since the asymptotic matching gives $g(\theta_d) + \mathrm{Ca} \ln(r/L_{\mathrm{out}}) = g(\Theta_i) + \mathrm{Ca} \ln(r/L_i)$. The second term of Eq. (2) is the static contribution to the interface shape which depends on the geometry of the system. The details of the asymptotic matching technique are beyond the scope of this work and we refer the interested reader to Cox [12] and Dussan V. *et al.* [18]. Physically, θ_d is the angle between the solid and the extrapolation of the outer, static interface back to the solid, see Fig. 1. It is clear from its definition that θ_d is not the interface slope at any particular location. In Eq. (2), θ_d is the only unknown. It may be determined experimentally by treating it as an adjustable parameter in a fit of Eq. (2) to experimental data of $\theta(r)$ at known Ca and L_{out}. Unlike the dissipation-based methods, by following this procedure we have explicit experimental proof that the model which leads to Eq. (1) correctly describes the fluid motion near the contact line before we even apply Eq. (1) to explore the inner physics.

Cox provides the simplest interpretation of L_i as the characteristic length (not necessarily a slip length) where the singularity is resolved [12]. In this framework, Θ_i is the contact angle boundary condition at the microscopic moving contact line. In a slightly more complex interpretation, L_i is the cutoff of the logarithmic divergence of the interface slope as $r/L_{\mathrm{out}} \to 0$. In this case, L_i need not be the characteristic length of the mechanism that resolves the singularity but the largest length scale where the usual assumptions cease to be valid [25,33]. Here, it could be possible for a cascade of physical mechanisms with successively smaller characteristic lengths $L_{i_1} > L_{i_2} > L_{i_3} \ldots$ to act at the contact line. If L_{i_1} is the length where the usual model first breaks down, then Θ_i is the interface slope associated with L_{i_1} [34]. Yet another interpretation of L_i is given in Cox's [35] posthumous paper on inertial effects on liquid spreading. The inner region is assumed to be resolved using a Navier slip model with slip length α. Unlike the conventional case of a slip condition at $\mathrm{Re} = 0$, where the inner length coincides with α, here a special definition of the inner length $L_i = \alpha^2 U/\nu$ (where ν is kinematic viscosity) is required in order to make the solution in the inner boundary layer independent of Re.

B. Using the model to analyze data

When we fit Eq. (2) to the measured interface shape, we check that Eq. (2) correctly describes the interface shape in the intermediate region, indicating that the flow has been modeled correctly. Then we may apply Eq. (1) knowing that we have connected to the inner region by using the correct flow in the intermediate region. In contrast, measuring θ_d directly from the extrapolated quasistatic shape $f_0(0;\theta_d)$ far from the contact line does provide the correct dynamic contact angle; however, this method does not establish anything about the physics of the flow near the contact line and, thus, poses a danger when it is used to infer inner dynamics.

Though not readily apparent, measurements of θ_d versus Ca contain information that allows one to probe some dynamics of Θ_i and L_i. The value of θ_d is made up of two dynamic contributions: first is the viscous deformation in the intermediate region, contained in the term Ca $\ln(L_{\text{out}}/L_i)$ in Eq. (1). We call this the "intermediate" contribution. The other dynamic component of θ_d comes from the possible dependences $\Theta_i(U)$ and $L_i(U)$. These dependences, which need not be scaled by Ca, constitute what we call the "inner" contribution.

In most cases reported in the literature, by far the largest of the two contributions is the intermediate one, wholly described by Ca. However, this need not always be the case. When A in the condition Ca $\ln \epsilon = -A$ as Ca$\to 0$ is small, the intermediate region where viscous bending is significant becomes vanishingly small. Then the interface shape looks static until it meets the inner region and $\theta_d = \Theta_i$. However, if in an experiment the viscous bending cannot be detected, the implications for the inner physics become ambiguous. Any one of the following might be happening. (i) The viscous bending is negligible but the inner contact angle $\Theta_i \neq \theta_s$ due to inner region dynamics, $\Theta_i(U)$. (ii) The viscous bending is negligible and $\Theta_i \approx \theta_s$. (iii) The viscous bending is not negligible but takes place in a region that is smaller than the spatial resolution of the experiment. Here the departure of θ_d from θ_s may be due to viscous bending, inner dynamics, or both.

When the intermediate contribution to θ_d is dominant, raw measurements of θ_d are relatively insensitive to material-dependent inner physics across material systems. This fact is often embodied in the well-known Hoffman curve where measurements of θ_d versus Ca on liquids with different θ_s moving in a capillary tube show a remarkable collapse [5]. Consequently, in order to expose the inner residual dynamic variation of θ_d, we must first subtract the dominant Ca-controlled intermediate contribution. This is discussed in the next section.

1. Exposing the inner region

Our goal is to learn about the dynamic dependence of L_i and Θ_i from measurements of θ_d versus U (or Ca). Since the dependence of L_i and Θ_i with U is unknown, we assume that they may be expanded in a Taylor series valid for small U as

$$L_i = L_0 + UL_1 + \cdots, \tag{3a}$$

$$\Theta_i = \theta_s + U\theta_1 + \cdots. \tag{3b}$$

L_0 represents the limit of L_i at zero spreading velocity. Clearly the use of a Taylor series may not include all cases since there is no guarantee that the powers must be integers. However, this assumption does not affect the value of L_0 which is one focus of our data analysis.

From Eqs. (1)–(3) it follows that in the small-U limit,

$$\begin{aligned} g(\theta_s) + \text{Ca}\,\ln\frac{L_{\text{out}}}{L_0} + U\theta_1\, g'(\theta_s) + U^2\left[\frac{1}{2}\theta_1^2\, g''(\theta_s) + \theta_2\, g'(\theta_s) - \frac{\mu}{\sigma}\frac{L_1}{L_0}\right] + U^3\left[\left(\frac{1}{2}L_1^2 - L_2 L_0\right)\frac{\mu}{\sigma L_0^2}\right. \\ \left. + \theta_3\, g'(\theta_s) + \theta_1\theta_2\, g''(\theta_s) + \frac{1}{6}\theta_1^3\, g'''(\theta_s)\right]\cdots \\ = g(\theta_d). \end{aligned}$$

When $\theta_s \neq 0$, even the O(1) term (made up of the first two terms on the left-hand side) has two unknowns. So we will only treat cases where $\theta_s = 0$, which reduces the above expression to

$$\begin{aligned} \text{Ca}\,\ln\frac{L_{\text{out}}}{L_0} - U^2\left(\frac{\mu L_1}{\sigma L_0}\right) + U^3\left[\left(\frac{1}{2}L_1^2 - L_2 L_0\right)\frac{\mu}{\sigma L_0^2} + \frac{\theta_1^3}{9}\right]\cdots \\ = g(\theta_d). \end{aligned} \tag{4}$$

To interpret data of θ_d versus Ca, Eq. (4) must be fitted to those data. From the terms proportional to U and U^2, we may extract L_0 and L_1. In the next section, we explain the details of this data analysis.

III. EXPERIMENTAL METHOD AND DATA ANALYSIS

In the experiments we immerse a vertical cylindrical Pyrex tube of radius $R_T = 1.25$ cm at constant velocity concentrically into a 10-cm-diam beaker filled with polydimethylsiloxane (PDMS) and we examine the shape of the meniscus that forms on the tube surface. We vary the chemistry of the tube surface and the molecular weight and end termination of the PDMS. Our range of molecular weights covers the entanglement limit (approximately at $\mu = 10$ P for PDMS) [36]. The Pyrex cleaning procedure, and optical and data acquisition systems are the same as used in previous studies [31]. The relative humidity is held below 6% in all experiments.

We compare measurements of the local interface slope, θ, versus distance to the contact line, r, to the theory, expressed in Eq. (2), that describes the dynamic interface shape near the moving contact line as $r/L_{\text{out}} \to 0$ [18]. All parameters in Eq. (2) are determined independently except θ_d. We extract θ_d for each material by fitting Eq. (2) to the measured interface shape at each spreading velocity U with θ_d as an adjustable fitting parameter. Since in our experiments the tube radius R_T is much larger than the capillary length a $[\equiv(\sigma/\rho g)^{1/2}]$, the appropriate outer length L_{out} for a tube immersed into a large liquid bath is a. A typical image appears in Fig. 2. A data set and fitting of Eq. (2) are shown in

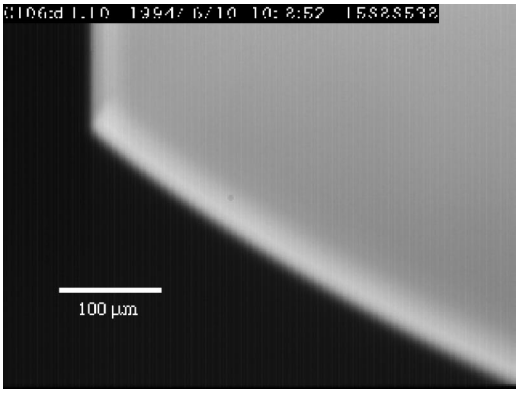

FIG. 2. The shadow of a meniscus advancing at $\mathrm{Ca} \approx 10^{-2}$.

Fig. 3. Using very strict statistical criteria, we only accept fits where χ^2 is statistically equivalent to 1 and there are no systematic deviations of the data from the model (resolving differences to less than 0.25°). We note that the variation of θ_d over the r range we probe does little more than translate the fitted curve along the θ axis while the curvature is fixed by Ca, which is independently determined. Thus, the success of the fit is a stringent test of the ability of the model to describe the viscous bending. The pixel noise in our camera produces an uncertainty in θ_d of about 0.1°. However, we see

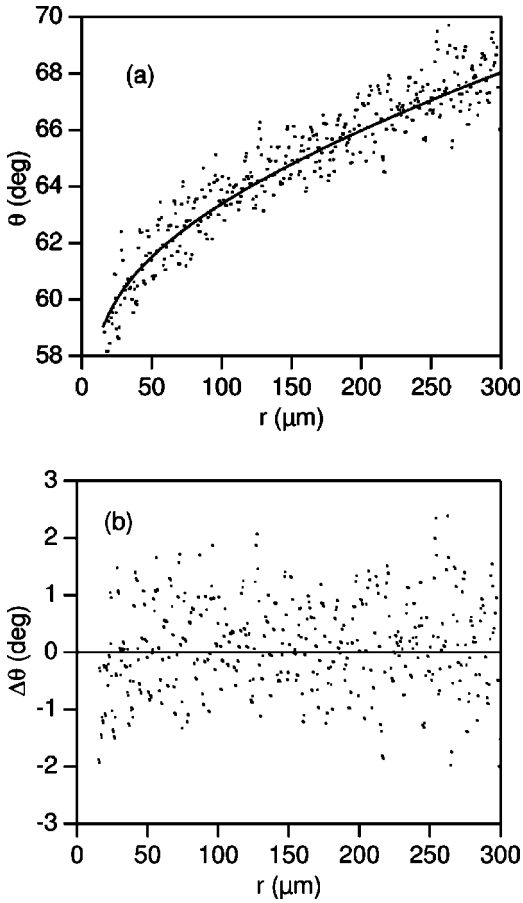

FIG. 3. $\mathrm{Ca} \approx 10^{-2}$. (a) Data (dots) and best fit ($\theta_d \approx 65°$) of Eq. (2) to the data. (b) Data minus best fit: difference is distributed uniformly around zero.

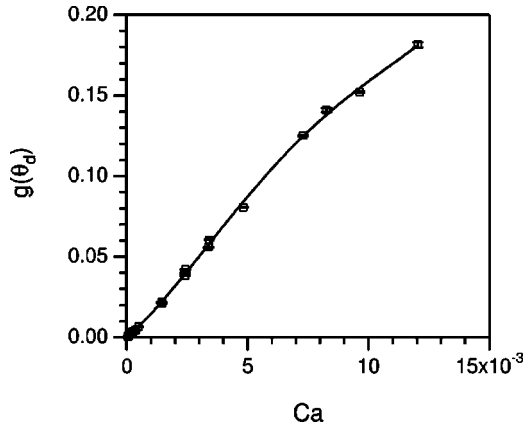

FIG. 4. Fit of $g(\theta_d)$ vs Ca using a fourth-degree polynimial. The system is 10 Poise, –OH-terminated PDMS spreading on silanated Pyrex.

larger variations among experiments performed under the same conditions but on repetitive cleanings of the same surface. These variations are reflected in the uncertainties on the data we report.

The basis for our data analysis is Eq. (4). Obviously if L_i and Θ_i were constants, then $\Theta_i = \theta_s = 0$ and $\{\theta_j = 0, L_j = 0 \text{ for } j \geq 1\}$, so that the quantity

$$G \equiv g(\theta_d) - \mathrm{Ca}\,\ln(a/L_0) \sim -U^2\left(\frac{\mu L_1}{\sigma L_0}\right) + U^3\left[\left(\frac{1}{2}L_1^2 - L_2 L_0\right)\frac{\mu}{\sigma L_0^2} + \frac{\theta_1^3}{9}\right] \quad (5)$$

would be zero. Thus, a departure from zero in the plot of G versus U (or Ca) indicates that at least one of L_i and Θ_i is velocity-dependent. We adopt this departure of G from 0 as a criterion to probe this velocity-dependent inner scale physics. The quantity G is more sensitive to the inner physics than $g(\theta_d)$ because it has most of the intermediate (i.e., "universal") dynamics stripped away.

Each series of $g(\theta_d)$ versus Ca is fitted to Eq. (1) using Eq. (3). The order of the polynomial in Eq. (3) is increased until the fit quality no longer improves as demonstrated by the F-test [37]. We find that, for the systems examined, between first- and fifth- order polynomials are required to fit the data. An example fit to a data set requiring fourth order is shown in Fig. 4. L_0 is extracted from the linear coefficient in such fits. If data were to be taken at higher speeds where Re cannot be neglected, it would be critical that the analysis be based on a modification of Eq. (1) accounting for the non-negligible effects of inertia on the fluid flows near the contact line [12,38].

Conventional studies of dynamic wetting focus on some version of a macroscopic dynamic contact angle and its variation with Ca for one or more classes of materials. Thus, graphs like that of Hoffman's [5] are obtained where the dynamic variation of the contact angle is mostly captured by the viscous hydrodynamic action of the "intermediate" region of the flow. This hydrodynamic action is "universal" in the sense that all its material dependence is accounted for by Ca. Figure 5 shows θ_d versus Ca for two PDMS of the same

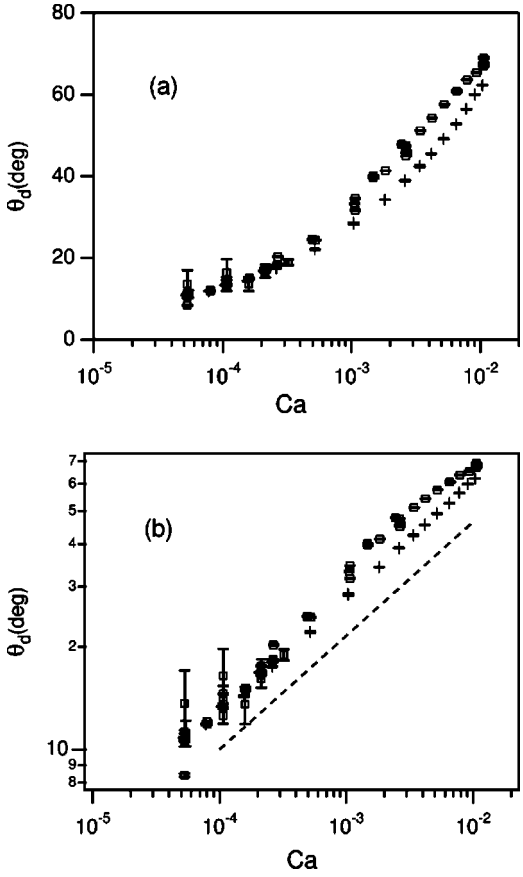

FIG. 5. θ_d vs Ca for two 10-Poise PDMS of different end termination. +: $-CH_3$; □: −OH. (a) linear-log; (b) log-log. Dashed line in (b) has slope 1/3.

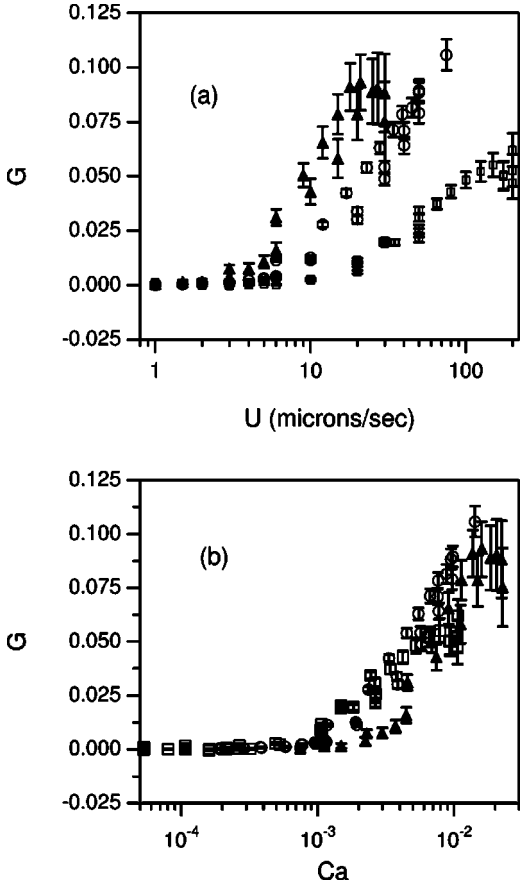

FIG. 7. G vs U (a) and G vs Ca (b) for the −OH terminated series. □: 10 Poise. ○: 40 Poise. ▲: 150 Poise.

viscosity (chain length) but different molecular end terminations, $-CH_3$ and −OH. Both the linear-log and the log-log plots show similar characteristics. In particular, both materials roughly follow a power law $Ca^{1/3}$. The level of differentiation in these results is similar to that seen in Hoffman's data.

When the universal contribution is stripped from the dynamic contact angle by forming the quantity G [cf. Eq. (5)], the residual dynamics of the inner region is exposed. Figure 6 shows that, for the two materials of Fig. 5, G departs statistically from zero. Thus, either one or both of the inner parameters, L_i and Θ_i, depend on U. While these effects become evident when the intermediate contributions to θ_d versus Ca are stripped away, the inner contribution remains small. Thus, imprecise methods of defining the dynamic contact angle and of measuring the contact angle could lead to systematic errors in derived inner scale parameters as well as

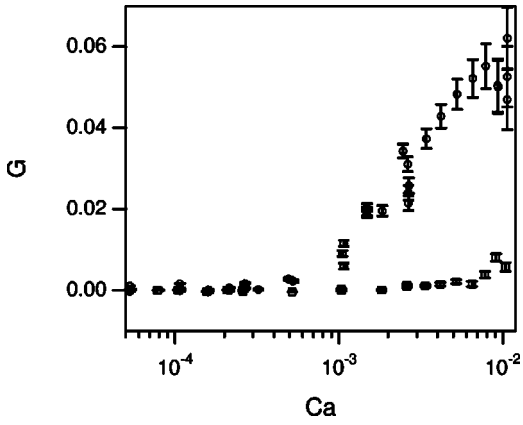

FIG. 6. G vs Ca for two 10-Poise PDMS fluids with different end termination spreading on bare Pyrex. □: $-CH_3$; ○: −OH. Error bars as marked or else smaller than marker size.

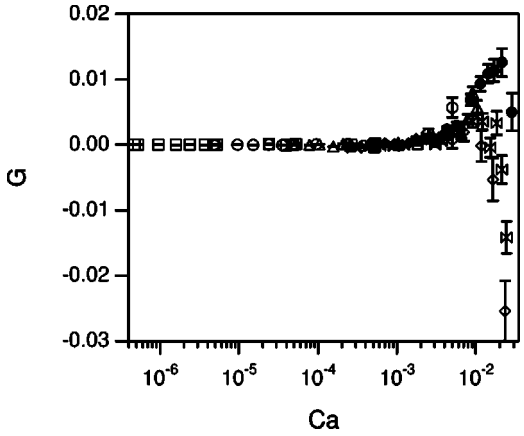

FIG. 8. G vs Ca for the $-CH_3$ terminated series. □: 10 cP. ○: 100 cP. △: 10 Poise. ◇: 50 Poise. ⋈: 120 Poise. ●: 600 Poise.

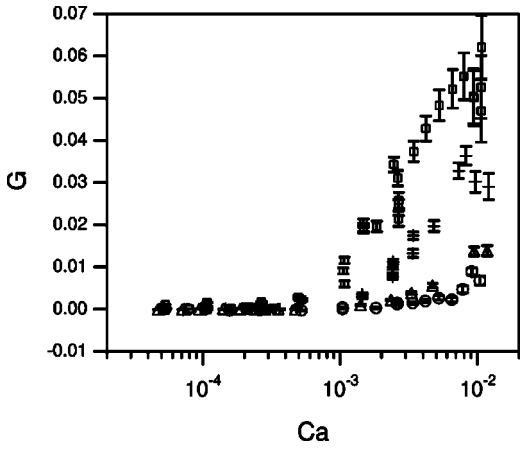

FIG. 9. Effect of surface for 10 Poise, −OH-terminated PDMS on □: bare Pyrex; +: silanated Pyrex; and for 10 Poise $-CH_3$-terminated PDMS on ○: bare Pyrex; △: silanated Pyrex.

in developing a boundary condition for the macroscopic interface [17].

IV. RESULTS AND DISCUSSION

In our materials studies, we change the liquid by using PDMS with two chain terminations ($-CH_3$ and −OH) and varying molecular weight/viscosity. We also alter the solid by surface modification (silanization). For all systems considered, $\theta_s=0$.

Besides the evidence that the inner parameters cannot be constants, Fig. 6 shows that (i) the dependence of the inner parameters on U is far from universal, and (ii) this dependence is not scaled by Ca. These results are shown for an entire series of fluids in Figs. 7(a) and 7(b), where G is plotted for the −OH series versus U and Ca. Using Ca instead of U does help contract the data cloud but is far from unifying the data. Thus, the inner dynamics is not wholly scalable by Ca even for such a simple material change as viscosity/chain length at fixed end termination. This lack of Ca scaling indicates that a new velocity scale must be present in the inner scale physics which, together with U, forms a dimensionless group that accounts for the U dependence of the inner parameters. Figures 7(b) and 8 show changes in inner region dynamics as a result of chain length variation for fixed molecule end group termination. Our $-CH_3$-terminated series shows effects as large as the −OH series, but we find that the contribution of the inner physics to the dynamic contact angle may be either positive or negative. The large effect of end termination on the inner dynamics of $\mu=10$ Poise PDMS is shown in Fig. 6, where two different inner dynamics can be seen. Similar differences are caused between the other pairs of closely matched viscosity oils with different end terminations.

Figure 9 compares dynamic inner effects for $-CH_3$- and −OH-terminated 10 Poise PDMS on two different surfaces: bare Pyrex and silanated Pyrex. By decreasing the polarity of the surface (silanization), the difference between −OH and $-CH_3$ is made smaller than in the bare Pyrex case. In addition, the difference between bare and silanated Pyrex is dramatic for the polar OH-terminated fluid, but almost nonexistent for the nonpolar CH_3-terminated fluid.

Having established that, according to the model of Eq. (1), at least one of the inner parameters must depend on U, we examine possible ramifications of the inner physics our

TABLE II. Effect of surface.

μ (cP)-end group	Surface	L_0 (nm)	U_c (μm/sec)	τ_c (ms)
1000-Methyl	bare Pyrex	3.7	40	0.92
1000-Methyl	silane	12	13	0.92
1000-OH	bare Pyrex	10	8	1.2
1000-OH	silane	4.7	3	1.6

TABLE I. Methyl and hydroxyl terminated PDMS on Pyrex.

μ (cP)	R_g[a] (nm)	L_0 (nm)	U_c (μm/sec)	τ_c (ms)	Chain length (monomer units)[b]
			Methyl		
10	1.3	3.6	>1000	<0.0036	17
100	2.8	1.5	100–400	0.0037–0.015	78
1000	9.5	3.7	40	0.92	870
5000	11	6.7	6	1.1	1200
12000	13	14	2	6.5	1600
60000	15	82	<1	>8.2	2000
			Hydroxyl		
1000	8.8	10	8	1.2	750
4000	11	300	2	150	1100
15000	13	270	1	270	1600

[a]See Ref. [36].
[b]Based on weight-average molecular weight.

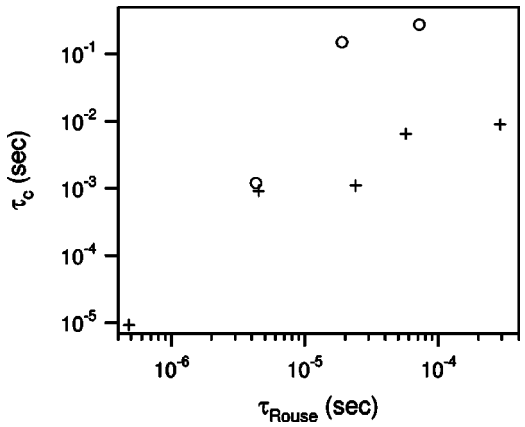

FIG. 10. τ_c vs Rouse relaxation time for each PDMS fluid used in this study. The entanglement limit occurs just before the data points at $\tau_c = 10^{-3}$ sec. +: CH_3; ○: OH.

measurements have revealed. In Tables I and II we list the values of L_0 found for all the systems. We see that L_0 is on the scale of the radius of gyration of the polymer. As shown in plots such as Figs. 7(b) and 8, each system has a critical speed, U_c, above which the inner parameters' velocity dependence becomes detectable. Below this critical velocity, the inner scale is L_0 and a residence time in the inner region is then $\tau \equiv L_0/U$ for $U < U_c$. Then the critical residence time, $\tau_c = L_0/U_c$ (i.e., the residence time above which the inner parameters exhibit their zero-U values), may be interpreted as an upper bound for a relaxation time of the inner physics, τ_{rel}. These values appear in Tables I and II.

Table I shows the following trends for systems on the same surface, bare Pyrex. (i) At fixed termination and increasing chain length, L_0 increases, U_c decreases, and τ_c increases. (ii) For fixed chain length, moving from −OH (polar end group polymer on a polar surface) to $-CH_3$ (a nonpolar end group polymer on a polar surface), L_0 decreases, U_c increases, and τ_c decreases. The decrease in τ_c may reflect a decrease in interaction of the $-CH_3$-terminated chain with the polar Pyrex surface compared to an −OH-terminated molecule of similar length. When we change surfaces, we see complex variations in L_0, U_c, and τ_c as we change the polarity of the surface and the polymer end termination (see Table II).

When $0 < U < U_c$, the inner parameters have their zero-U values, viz., $L_i = L_0$ and $\Theta_i = 0$. This implies that $\tau_{\mathrm{rel}} < \tau_c < \tau$ so that the molecule is completely relaxed as it exits L_0. Comparing τ_c to a relaxation time in the bulk polymer, the Rouse relaxation time τ_{Rouse} [39–41], Fig. 10 shows a jump in τ_c from below to above the entanglement limit. Further, τ_c correlates with τ_{Rouse} above the entanglement limit with different correlations for each end group.

Above the critical speed, things are less well defined. However, we can safely say that, since $L_1 > 0$ for all our fittings, then $L_i = L_0 + UL_1 > L_0$ at $U > U_c$, i.e., L_i increases with U at small enough U. This scenario would be consistent with Shikhmurzaev's ideas [27] where L_i is the length required to relax an interphase layer of molecular thickness having a fixed relaxation time, $\tau_{\mathrm{rel}} \equiv L_i/U$. According to Shikhmurzaev, the layer would exit L_i completely relaxed to enter the region where the usual hydrodynamic assumptions hold. In this view, L_i would also be an increasing function of U.

V. SUMMARY

We note that the theory behind Eq. (1) does not require Θ_i and L_i to be constant, thus allowing these quantities to depend on U. Using a phenomenological dependence for Θ_i and L_i, we formulated a method for analyzing data of θ_d versus Ca that allows us to detect when this dependence demands that either or both Θ_i and L_i be functions of U.

Analysis of our experimental data shows that, for our material systems, at least one of Θ_i and L_i must depend on U. This dependence becomes detectable above a certain critical spreading velocity, U_c. In addition, the data show that a precise definition and determination of θ_d is essential for getting the correct inner dynamics. We do this by verifying that the model which includes Eq. (1) precisely describes the viscous deformation on the interface near the contact line [cf. Eq. (2)].

Far from contradicting the model, allowing Θ_i and L_i to depend on U endows the model with a richer set of dynamics affecting θ_d. Since Θ_i and L_i depend on U through a parameter other than Ca, this demands a new time scale (or velocity scale) in the model of the inner region, possibly related to a relaxation time of the fluid. This finding is consistent with theories such as Shikhmurzaev's, where the actual dynamic contact angle Θ_i is a complex function of the flow via its dependence on the interfacial energies of all interphase regions meeting at the contact line, and the inner length L_i is an increasing function of U. Attempts at extracting such a time scale from our data show systematic trends across materials and molecular weights.

ACKNOWLEDGMENTS

We are grateful for NASA's support through Grants No. NAG3-2449 and No. NCC3-465. We are also most grateful to Gita Seevaratnam for her help with evaluating the Rouse relaxation times.

[1] E. B. Dussan V., Annu. Rev. Fluid Mech. **11**, 371 (1979).
[2] S. F. Kistler, in *Wettability*, edited by J. C. Berg, Vol. 49 of Surfactant Science (Marcel Dekker, New York, 1993), pp. 311–429.
[3] T. D. Blake, in *Wettability* (Ref. [2]), pp. 251–309.
[4] C. G. Ngan and E. B. Dussan V., J. Fluid Mech. **209**, 191 (1989).
[5] R. L. Hoffman, J. Colloid Interface Sci. **50**, 228 (1975).

[6] E. B. Gutoff and C. E. Kendrick, AIChE J. **50**, 459 (1982).
[7] J. E. Seebergh and J. C. Berg, Chem. Eng. Sci. **47**, 17 (1992).
[8] E. B. Dussan V., J. Fluid Mech. **77**, 665 (1976).
[9] L. M. Hocking, J. Fluid Mech. **79**, 209 (1977).
[10] C. Huh and S. G. Mason, J. Fluid Mech. **81**, 401 (1977).
[11] D. E. Weidener and L. W. Schwartz, Phys. Fluids **6**, 3535 (1994).
[12] R. G. Cox, J. Fluid Mech. **168**, 169 (1986).
[13] L. M. Hocking and A. D. Rivers, J. Fluid Mech. **121**, 425 (1982).
[14] L. M. Pismen and A. Nir, Phys. Fluids **25**, 3 (1982).
[15] H. P. Kavehpour, B. Ovryn, and G. H. McKinley, Phys. Rev. Lett. **91**, 196104 (2003).
[16] X. Chen, E. Ramé, and S. Garoff, Phys. Fluids **16**, 287 (2004).
[17] J. A. Marsh, S. Garoff, and E. B. Dussan V., Phys. Rev. Lett. **70**, 2778 (1993).
[18] E. B. Dussan V., E. Ramé, and S. Garoff, J. Fluid Mech. **230**, 97 (1991).
[19] P. A. Thompson and M. O. Robbins, Phys. Rev. Lett. **63**, 766 (1989).
[20] J. Koplik, J. R. Banavar, and J. F. Willemsen, Phys. Rev. Lett. **60**, 1282 (1988).
[21] N. G. Hadjiconstantinou, Phys. Rev. E **59**, 2475 (1999); **69**, 069901(E) (2004).
[22] F. Gentner, G. Ogonowski, and J. de Coninck, Langmuir **19**, 3996 (2003).
[23] W. Jin, J. Koplik, and J. R. Banavar, Phys. Rev. Lett. **78**, 1520 (1997).
[24] H.-Y. Chen, D. Jasnow, and J. Viñals, Phys. Rev. Lett. **85**, 1686 (2000).
[25] J. Eggers and H. Stone, J. Fluid Mech. **505**, 309 (2004).
[26] M. J. de Ruijter, J. de Coninck, T. D. Blake, A. Clarke, and A. Rankin, Langmuir **13**, 7293 (1997).
[27] Y. D. Shikhmurzaev, Int. J. Multiphase Flow **19**, 589 (1993).
[28] Y. D. Shikhmurzaev, J. Fluid Mech. **334**, 211 (1997).
[29] P.-G. de Gennes, Rev. Mod. Phys. **57**, 827 (1985).
[30] M. J. de Ruijter, J. de Coninck, and G. Oshanin, Langmuir **15**, 2209 (1999).
[31] Q. Chen, E. Ramé, and S. Garoff, Phys. Fluids **7**, 2631 (1995).
[32] T. D. Blake, M. Bracke, and Y. D. Shikhmurzaev, Phys. Fluids **11**, 1995 (1999).
[33] P.-G. de Gennes, X. Hua, and P. Levinson, J. Fluid Mech. **212**, 55 (1990).
[34] E. Ramé, in *Encyclopedia of Surface and Colloid Science*, edited by A. Hubbard (Marcel Dekker, New York, 2002), pp. 3602–3618.
[35] R. G. Cox, J. Fluid Mech. **357**, 249 (1998).
[36] K. R. Willson, Ph.D. thesis, Carnegie Mellon University, 1995.
[37] P. R. Bevington and D. K. Robinson, *Data Reduction and Error Analysis for the Physical Sciences*, 2nd ed. (McGraw Hill, Boston, 1979), pp. 205–209.
[38] K. Stoev, E. Ramé, and S. Garoff, Phys. Fluids **11**, 1995 (1999).
[39] G. C. Berry and D. J. Plazek, in *Glass: Science and Technology*, edited by N. J. Kreidl and D. R. Uhlmann, Materials Science and Technology Vol. 3: Viscosity and Relaxation (Academic, Orlando, 1986), pp. 319–362.
[40] G. C. Berry, in *Desk Reference of Polymer Characterization and Analysis*, edited by J. F. Brady (American Chemical Society, New York, 2000), Chap. 6, pp. 35–43.
[41] E. F. Casassa, in *Comprehensive Polymer Science*, edited by G. Allen (Pergamon, New York, 1988), Vol. 2, Chap. 3.
[42] When $\theta \ll 1$, $\theta_d^3 - \Theta_i^3 = 9\ \mathrm{Ca}\ \ln(L_{\mathrm{out}}/L_i)$. If $\Theta_i = 0$ and $L_i = \mathrm{const}$, the familiar power law, $\theta_d \sim \mathrm{Ca}^{1/3}$, is obtained.